

Published in final edited form as:

*Neuroimage*. 2012 March ; 60(1): 1–6. doi:10.1016/j.neuroimage.2011.11.091.

## Imaging acute ischemic tissue acidosis with pH-sensitive endogenous amide proton transfer (APT) MRI - Correction of tissue relaxation and concomitant RF irradiation effects toward mapping quantitative cerebral tissue pH

Phillip Zhe Sun, PhD<sup>1,\*</sup>, Enfeng Wang, MD<sup>1</sup>, and Jerry S Cheung, PhD<sup>1</sup>

<sup>1</sup>Athinoula A. Martinos Center for Biomedical Imaging, Department of Radiology, Massachusetts General Hospital and Harvard Medical School, Charlestown MA 02129

### Abstract

Amide proton transfer (APT) MRI is sensitive to ischemic tissue acidosis and has been increasingly used as a research tool to investigate disrupted tissue metabolism during acute stroke. However, magnetization transfer asymmetry ( $MTR_{\text{asym}}$ ) analysis is often used for calculating APT contrast, which only provides pH-weighted images. In addition to pH-dependent APT contrast, *in vivo*  $MTR_{\text{asym}}$  is subject to a baseline shift ( $\Delta MTR'_{\text{asym}}$ ) attributable to the slightly asymmetric magnetization transfer (MT) effect. Additionally, APT contrast approximately scales with  $T_1$  relaxation time. Tissue relaxation time may also affect the experimentally obtainable APT contrast via saturation efficiency and RF spillover effects. In this study, we acquired perfusion, diffusion, relaxation and pH-weighted APT MRI data, and spectroscopy (MRS) in an animal model of acute ischemic stroke. We modeled *in vivo*  $MTR_{\text{asym}}$  as a superposition of pH-dependent APT contrast and a baseline shift  $\Delta MTR'_{\text{asym}}$  (i.e.,  $MTR_{\text{asym}} = APTR(\text{pH}) + \Delta MTR'_{\text{asym}}$ ), and quantified tissue pH. We found pH of the contralateral normal tissue to be  $7.03 \pm 0.05$  and the ipsilateral ischemic tissue pH was  $6.44 \pm 0.24$ , which correlated with tissue perfusion and diffusion rates. In summary, our study established an endogenous and quantitative pH imaging technique for improved characterization of ischemic tissue acidification and metabolism disruption.

### Keywords

acute stroke; amide proton transfer (APT); chemical exchange saturation transfer (CEST); MRI; pH; tissue acidosis

## 1. Introduction

Ischemic tissue undergoes a complex cascade of hemodynamic, metabolic and molecular disturbances during acute ischemic stroke—among them, altered glucose and oxygen metabolism, tissue acidification, adenosine triphosphate (ATP) depletion and ultimately

© 2011 Elsevier Inc. All rights reserved.

\*Corresponding Author: Phillip Zhe Sun, Ph.D. 149 13th Street, Rm 2301, Athinoula A. Martinos Center for Biomedical Imaging, Department of Radiology, MGH and Harvard Medical School, Charlestown, MA 02129, pzhesun@nmr.mgh.harvard.edu, Phone: 617-726-4060; Fax: 617-726-7422.

**Publisher's Disclaimer:** This is a PDF file of an unedited manuscript that has been accepted for publication. As a service to our customers we are providing this early version of the manuscript. The manuscript will undergo copyediting, typesetting, and review of the resulting proof before it is published in its final citable form. Please note that during the production process errors may be discovered which could affect the content, and all legal disclaimers that apply to the journal pertain.

infarction (Astrup et al., 1981; Hossmann, 1994; Siesjo, 1992). Because perfusion and diffusion MRI (PWI/DWI) can characterize tissue hemodynamic and structural status, they have been increasingly used to study acute stroke, both in preclinical research and clinical care (Moseley et al., 1990; Schaefer et al., 2003; Schlaug et al., 1999). In addition, the PWI/DWI mismatch has been postulated as a surrogate imaging marker for salvageable ischemic tissue (penumbra) to guide stroke treatment beyond the narrow thrombolytic window (Marks et al., 2008; Warach, 2002). However, ischemic tissue damage is heterogeneous and the PWI/DWI mismatch only provides a crude approximation of the penumbra (Kidwell et al., 2004). Therefore, it is important to develop complementary neuroimaging techniques to better stratify ischemic tissue for treatment (Kloska et al., 2010; Rivers et al., 2006). Toward this goal, we have been investigating tissue pH as a potential new imaging parameter. Specifically, ischemic tissue becomes acidic upon initiation of anaerobic respiration and elevation of lactate concentration (Paschen et al., 1992). The hypoperfusion and reduced buffering capacity of bicarbonate at acidic pH further disrupt tissue metabolism, which aggravates tissue acidosis (Zauner et al., 2002). Because reasonably preserved energy metabolism and pH are vital for cell viability, it is important to study tissue acidosis in addition to perfusion and diffusion for improved characterization of ischemic tissue damage.

It has been shown with histology that acidosis is associated with ATP depletion and abnormal protein synthesis, and is a surrogate marker for disrupted tissue metabolism (Hata et al., 1998; Höhn-Berlage et al., 1989). Magnetic resonance spectroscopy (MRS) has been used to assess key tissue metabolites and pH during stroke (Bolas et al., 1988; Nicoli et al., 2003; Parsons et al., 2000). However, further technical development of MRS is needed to enhance its spatiotemporal resolution so it can be routinely used to study fast evolving acute stroke. More recently, amide proton transfer (APT) imaging, a form of chemical exchange saturation transfer (CEST) MRI, has been shown to be sensitive to pH and mobile proteins/peptides content with significantly higher spatiotemporal resolution than spectroscopy (Jokivarsi et al., 2007; Mougín et al., 2010; Sun et al., 2007b; Ward and Balaban, 2000; Zhou et al., 2003). In vivo APT MRI contrast is often calculated using the magnetization transfer (MT) asymmetry analysis ( $MTR_{\text{asym}}$ ), which is complex due to relaxation and concomitant RF irradiation effects. APT contrast approximately scales with  $T_1$  relaxation time. In addition to the pH-dependent APT contrast,  $MTR_{\text{asym}}$  is susceptible to slightly asymmetric magnetization transfer effects (Hua et al., 2007; Pekar et al., 1996). Moreover, the experimentally obtained CEST MRI contrast strongly varies with RF irradiation power, which can be described using the saturation/labeling coefficient and RF spillover effects.

We postulated that tissue pH can be reasonably quantified from pH-weighted APT MRI by taking into account major concomitant RF irradiation effects. Specifically, we characterized acute ischemic tissue damage with multi-parametric MRI and point resolved spectroscopy (PRESS) using a filament middle cerebral artery occlusion (MCAO) animal model of acute ischemic stroke. We modeled the in vivo  $MTR_{\text{asym}}$  contrast as a superposition of pH-dependent APT contrast (APTR) and MT asymmetry-induced baseline shift ( $\Delta MTR'_{\text{asym}}$ ), and numerically solved tissue pH using the base-catalyzed amide proton exchange rate relationship. Our study showed that APT MRI is indeed capable of measuring tissue pH, which correlates with perfusion and diffusion deficit. In summary, development of quantitative pH imaging from pH-weighted APT MRI allows more specific characterization of tissue acidosis, which may improve the stratification of heterogeneous ischemic tissue damage and ultimately, a better guide for stroke treatment.

## 2. Material and Methods

### 2.1 Animal Model

All experiments were approved by the Institutional Subcommittee on Research Animal Care, Massachusetts General Hospital (SRAC, MGH). Adult male Wistar rats (n=12, Charles River Laboratory, Wilmington, MA) were anesthetized with 1.5–2% isoflurane in air during surgery and MRI. We scanned the animals approximately 1 hr after filament MCAO. The animals' core temperature was maintained, with heart rate and blood oxygen saturation (SpO<sub>2</sub>) monitored online (Nonin Pulse Oximeter 8600, Plymouth, MN).

### 2.2 Simulation

pH-weighted CEST MRI contrast can be described by a 2-pool exchange model (Sun et al., 2007b),

$$\text{CESTR} = \frac{f_s \cdot k_{sw}}{R_{1w} + f_s \cdot k_{sw}} \cdot \alpha \cdot (1 - \sigma) \quad (1)$$

where  $\alpha$  is the labeling coefficient and  $\sigma$  is the spillover factor;  $k_{sw}$  is pH-dependent amide proton exchange rate,  $f_s$  is the labile amide proton concentration with respect to bulk water, and  $R_{1w}$  is the bulk water longitudinal relaxation rate. For slow chemical exchange, we have

$$\alpha = \frac{\omega_1^2}{p \cdot q + \omega_1^2} \quad \text{and} \quad \sigma = 1 - \frac{r_{1w}}{k_{ws}} \left( \frac{R_{1w}r_{zs}\cos^2\theta + R_{1s}k_{ws}\cos\theta\cos^2(\theta/2)}{r_{zw}r_{zs} - k_{ws}k_{sw}\cos^2(\theta/2)} - \frac{R_{1w}r_{2s}\cos^2\theta}{r_{zw}r_{2s} - k_{ws}k_{sw}\sin^2\theta} \right)$$

where  $p = r_{2s} - \frac{k_{sw}k_{ws}}{r_{2w}}$ ,  $q = r_{1s} - \frac{k_{sw}k_{ws}}{r_{1w}}$ ,  $r_{zw} = r_{1w}\cos^2\theta/2 + r_{2w}\sin^2\theta/2$ ,  $r_{zs} = r_{1s}\cos^2\theta + r_{2s}\sin^2\theta$ ,  $r_{1w,s} = R_{1w,s} + k_{ws,sw}$ ,  $r_{2w,s} = R_{2w,s} + k_{ws,sw}$  and  $\theta = \tan^{-1}(\omega_1/\Delta\omega_s)$ . We used typical cerebral tissue relaxation time at 4.7 Tesla:  $T_{1w}=1.5$  s,  $T_{2w}=56$  ms,  $T_{1s}=1$  s,  $T_{2s}=15$  ms and  $\Delta\omega_s=3.5$  ppm. In addition, the relative labile proton concentration with respect to water protons was assumed to be 1:850 (Sun et al., 2007b), and the amide proton exchange rate was estimated using  $k_{sw} = 5.57 \cdot 10^{\text{pH}-6.4}$  (Zhou et al., 2003).

### 2.3 Data Acquisition

Animals were imaged using a 4.7 Tesla small bore Bruker MRI scanner (Bruker Biospec, Billerica, MA) (Sun et al., 2011b). Water-suppressed <sup>1</sup>H PRESS MRS data were acquired from a cubic region of interest (ROI) of 3.5×3.5×3.5 mm<sup>3</sup> positioned in the striatum, with an acquisition time of about 17 min (repetition time (TR)/echo time (TE)=2,000/144 ms, number of average (NA)=512). Multi-parametric MRI was obtained with single-shot echo planar imaging (EPI) (field of view: 25×25 mm<sup>2</sup>, matrix: 64×64, 5 slices, slice thickness = 2mm, bandwidth 200 kHz). Seven T<sub>1</sub>-weighted images were acquired for T<sub>1</sub> mapping using an inversion recovery sequence, with their inversion delays ranging from 250 ms to 3000 ms (TR/TE=6500/14.8 ms, NA=4). Two T<sub>2</sub>-weighted images were obtained for T<sub>2</sub> mapping with TEs of 30 and 100 ms (TR=3250 ms, NA=16). Single-shot diffusion-weighted MRI was acquired with two b-values of 250 and 1000 s/mm<sup>2</sup> (TR/TE=3250/54ms, NA=16). We also acquired perfusion images with arterial spin labeling (ASL) (TR/TE=6500ms/28ms, NA=32, time of saturation (TS)=3000 ms) (Alsop and Detre, 1998; Utting et al., 2005). For pH-weighted APT MRI, we set the recovery time to 5000 ms, primary RF saturation duration (TS<sub>1</sub>=4500ms), and secondary RF saturation duration (TS<sub>2</sub>=500 ms) for an RF irradiation amplitude of 0.75 μT applied at ±3.5ppm (Sun et al., 2011a). The control scan was signal-averaged 8 times, while the saturated images were averaged 32 times.

## 2.4 Data Processing

We processed the MRS spectra with java-based Magnetic Resonance User Interface (jMRUI v4.0, <http://www.mrui.uab.es/mrui/>), as described previously (Sun et al., 2011b). MRI images were processed in Matlab (Mathworks, Natick, MA). We obtained parametric  $T_1$ ,  $T_2$  and apparent diffusion coefficient (ADC) maps using least-squares mono-exponential fitting of the signal intensities as functions of inversion time ( $I = I_0[1 - (1 - \eta)e^{-TI/T_1}]$ ), where  $\eta$  is the inversion efficiency, echo time ( $I = I_0e^{-TE/T_2}$ ), and diffusion b-value ( $I = I_0e^{-b \cdot ADC}$ ),

respectively. Cerebral blood flow (CBF) was calculated as  $CBF = \frac{\lambda}{T_{1app}} \cdot \frac{I_{ref} - I_{tag}}{2\alpha \cdot I_{ref}}$ , where  $\lambda$  is the brain/blood partition coefficient,  $\alpha$  is the degree of inversion,  $I_{tag}$  and  $I_{ref}$  are ASL tagging and reference images, respectively, and  $T_{1app}$  is the longitudinal relaxation time in the presence of RF labeling pulse. We assumed  $\lambda = 0.9$  ml/g,  $\alpha = 0.63$  and  $T_{1app} = 0.84$  s (Utting et al., 2005).

In vivo MTR asymmetry ( $MTR_{asym}$ ) was calculated as  $MTR_{asym} = (I_{ref} - I_{label})/I_0$ , where  $I_{label}$  and  $I_{ref}$  are the APT label and reference images, and  $I_0$  is the control image without RF saturation. In vivo  $MTR_{asym}$  can be described as a superposition of APTR and  $\Delta MTR'_{asym}$ :

$$\begin{aligned} MTR_{asym} &= \Delta MTR'_{asym} + APTR \\ &= \Delta MTR'_{asym} + \frac{f_s \cdot k_{sw}}{R_{1w} + f_s \cdot k_{sw}} \cdot \alpha \cdot (1 - \sigma) \end{aligned} \quad (2)$$

Because  $\alpha$  and  $\sigma$  were reasonably constant as a function of the chemical exchange rate (Fig. 1), they were estimated assuming a mean amide proton exchange rate of  $20 \text{ s}^{-1}$ . We used the mean  $T_1$  and  $T_2$  values of the ipsilateral ischemic ROI. The exchange rate can be solved as

$$k_{sw} = \frac{R_{1w}}{f_s \left( \frac{\alpha \cdot (1 - \sigma)}{MTR_{asym} - \Delta MTR'_{asym}} - 1 \right)} \quad (3)$$

Because the regional brain  $T_1$  and  $T_2$  difference may be beyond that observed in the ipsilateral ROI,  $\alpha$  and  $\sigma$  parametric maps were calculated using  $T_1$  and  $T_2$  maps for pH mapping. We used numerically solved  $f_s$  and  $\Delta MTR'_{asym}$ , and pH map was derived using the base-catalyzed amide proton exchange relationship (Zhou et al., 2003).

$$\begin{aligned} pH &= 6.4 + \log_{10}(k_{sw}/5.57) \\ &= 6.4 + \log_{10} \left( \frac{R_{1w}}{f_s \left( \frac{\alpha \cdot (1 - \sigma)}{MTR_{asym} - \Delta MTR'_{asym}} - 1 \right)} / 5.57 \right) \end{aligned} \quad (4)$$

## 3. RESULTS

Fig. 1 plots pH-sensitive APT MRI contrast. Fig. 1a shows base-catalyzed amide proton exchange rate as a function of pH,  $k_{sw} = 5.57 \times 10^{\text{pH}-6.4}$  (Zhou et al., 2003). Because the exchange rate is slow ( $10\text{--}30 \text{ s}^{-1}$ ) at physiological pH, the labeling coefficient and spillover factors are reasonably constant (Figs. 1 b and c). For  $B_1 = 0.75 \text{ } \mu\text{T}$ , we have  $\alpha = 0.97 \pm 0.02$  and  $1 - \sigma = 0.90 \pm 0.001$  (solid line) for the typical range of tissue pH, and for  $B_1 = 1.5 \text{ } \mu\text{T}$ , we have  $\alpha = 0.99 \pm 0.01$  and  $1 - \sigma = 0.68 \pm 0.002$  (dashed line). The dominantly base-catalyzed amide proton exchange process confers pH sensitivity to APT MRI, with image contrast increasing with pH (Fig. 1d). It is important to note that APT contrast depends on the RF

irradiation power. The use of 1.5  $\mu\text{T}$  induces significantly more RF spillover effects, resulting in less CEST contrast than that of 0.75  $\mu\text{T}$  (solid line). This is consistent with our previous finding that 0.75  $\mu\text{T}$  is approximately the optimal RF power for APT imaging of acute stroke at 4.7 Tesla, which we used in our in vivo study (Sun et al., 2007b).

Fig. 2 shows multi-parametric MRI of a representative acute stroke rat. Ischemic tissue displayed severe CBF (Fig. 2a), pH-weighted  $\text{MTR}_{\text{asym}}$  (Fig. 2b) and ADC (Fig. 2c) deficits. Lactate was measured from an ROI positioned in the ipsilateral striatum, while CBF, pH-weighted MTR asymmetry and ADC were obtained from both the ipsilateral ischemic ROI and the contralateral normal ROI. The ischemic ROI was positioned in striatum, which often displays severe ischemic damage. Specifically, the ischemic lesion showed elevated lactate signal, with a Choline and Creatine normalized lactate peak (i.e.,  $\text{Lac}/(\text{Cho}+\text{Cr})$ ) being  $0.80 \pm 0.21$ . CBF decreased from  $2.3 \pm 0.54$  ml/g.min in the contralateral normal area to  $1.13 \pm 0.57$  ml/g.min in the ischemic lesion, representing a relative decrease of  $52 \pm 19\%$  ( $P < 0.01$ ). pH-weighted  $\text{MTR}_{\text{asym}}$  was  $-4.3 \pm 0.3\%$  in the contralateral normal ROI, which decreased to  $-6.1 \pm 0.6\%$  upon ischemia ( $P < 0.01$ ). In addition, ADC decreased from  $0.72 \pm 0.03$  to  $0.56 \pm 0.03$   $\mu\text{m}^2/\text{ms}$  ( $P < 0.01$ ). The relatively small standard deviation of ischemic lesion ADC suggests the consistency of MCAO surgery and ROI selection.

The ipsilateral ischemic ROI-based  $\text{MTR}_{\text{asym}}$  is plotted as a function of pH in Fig. 3. The lactate concentration [Lac] was calculated from PRESS MRS, with Creatine and Choline concentration being 4.79 and 9.35 mmol/kg, respectively, according to Florian et al. (Florian et al., 1996). Tissue pH was estimated from the lactate concentration at  $\text{pH} = -0.0593 \cdot [\text{Lac}] + 7.2$ , following the results of Chang et al. (Chang et al., 1990). Unlike the calculated amide proton CEST contrast (Fig. 1), in vivo  $\text{MTR}_{\text{asym}}$  was negative due to the baseline shift of  $\Delta\text{MTR}'_{\text{asym}}$ . Because  $\alpha$  and  $\sigma$  are reasonably constant for slow chemical exchange, we assumed a mean amide proton exchange rate of  $20 \text{ s}^{-1}$ , and used the mean  $T_1$  (1.63 s) and  $T_2$  (55 ms) from the ipsilateral ROI to calculate  $\alpha$  and  $\sigma$ .  $K_{\text{sw}}$  was calculated using  $k_{\text{sw}} = 5.57 \times 10^{\text{pH}-6.4}$  and two parameters,  $\Delta\text{MTR}'_{\text{asym}}$  and  $f_s$ , were numerically solved from Eq. 2, being  $-7.44\%$  and 1:867, respectively. It is important to note that the numerically solved  $f_s$  was in good agreement with that derived from the dual 2-pool exchange model in a previous study (Sun et al., 2007b). In addition, we calculated the contralateral normal tissue pH from quantitative APT MRI (Eq. 4), and overlaid its  $\text{MTR}_{\text{asym}}$  in Fig. 3 (open squares). This shows that the proposed quantitative pH MRI can reasonably describe in vivo APT MRI contrast.

Fig. 4 shows the calculation of quantitative tissue pH map from pH-weighted APT MRI. The ischemic lesion showed subtle changes in  $T_1$  and  $T_2$  maps (Figs. 4 a and b).  $T_1$  increased from  $1.53 \pm 0.06$  s of the contralateral normal area to  $1.63 \pm 0.07$  s of the ipsilateral region ( $P < 0.01$ ) while the  $T_2$  decreased from  $56.4 \pm 2$  ms to  $55.0 \pm 1.1$  ms ( $P < 0.01$ ). Whereas the computed labeling coefficient map is reasonably homogeneous (Fig. 4 c), there is noticeable heterogeneity in the spillover factor map (Fig. 4 d). This is because the regional brain  $T_1$  and  $T_2$  difference may be beyond the change observed in the ipsilateral ischemic ROI, and calculation of parametric  $\alpha$  and  $\sigma$  maps is needed to improve pH quantification. Fig. 4e shows the pH-weighted  $\text{MTR}_{\text{asym}}$  map. Because it has been shown that cerebral tissue  $R_{1w}$  increases with the MT contrast,  $R_{1w}$ -scaled  $\Delta\text{MTR}'_{\text{asym}}$  map (Fig. 4f) was calculated (i.e.,  $\Delta\text{MTR}'_{\text{asym}} = -7.44\% \cdot R_{1w}/R_{1w\_ipsi} = -7.44\% \cdot 1.63/T_{1w}$ ). Specifically,  $-7.44\%$  was obtained from numerical fitting (Fig. 3) with  $T_{1w\_ipsi}$  being  $T_{1w}$  of the ipsilateral ROI (1.63 s). This effectively compensated the hypointensity over corpus callosum in the  $\text{MTR}_{\text{asym}}$  map. Fig. 4g shows the endogenous APT map (i.e.,  $\text{APTR} = \text{MTR}_{\text{asym}} - \Delta\text{MTR}'_{\text{asym}}$ ), which displays acidosis-induced deficit. pH was determined from the measured  $\text{MTR}_{\text{asym}}$  map (Eq. 4), with  $f_s$  and  $\Delta\text{MTR}'_{\text{asym}}$  assumed

independent of pH and equal to the results determined in Fig. 3. Note that whereas  $\alpha$  and  $\sigma$  are relatively constant as a function of pH, it is necessary to estimate the experimental factor per voxel (i.e.,  $\alpha^*(1-\sigma)$ ) for quantifying the regional tissue pH. Indeed, the pH map derived from Eq. 4 clearly depicts tissue acidification in the ischemic lesion (Fig. 4 h). Ischemic tissue pH estimated from APT MRI was  $6.44 \pm 0.24$ , in good agreement with that estimated from lactate MRS of  $6.53 \pm 0.18$ . In comparison, the contralateral normal tissue pH was  $7.03 \pm 0.05$ , and the pH difference between the ischemic and contralateral normal regions was  $-0.59 \pm 0.22$  ( $P < 0.01$ ). We also evaluated the association between ischemic tissue pH and its perfusion and diffusion rates. Fig. 5 a shows that ischemic tissue pH correlates with the residual CBF, which can be described by a linear regression relationship,  $\text{CBF} = 1.61 * \text{pH} - 9.22$  ml/g.min ( $R^2 = 0.46$ , Significance  $F < 0.02$ ). In addition, tissue pH correlates with ADC (Fig. 5 b), with  $\text{ADC} = 0.090 * \text{pH} - 0.02$   $\mu\text{m}^2/\text{ms}$  ( $R^2 = 0.45$ , Significance  $F < 0.02$ ).

#### 4. Discussion

Our study quantified pH-weighted in vivo APT MRI contrast for absolute tissue pH mapping and characterized ischemic tissue acidification. Given that CEST/APT MRI contrast approximately scales with  $T_1$ , we designed our in vivo study to acquire multi-parametric MRI so we can take that into account, which should improve the specificity and accuracy of cerebral tissue pH mapping. We also estimated the labeling coefficient and spillover factor to correct for concomitant RF irradiation effects. In fact, after correcting the intrinsic  $\Delta\text{MTR}'_{\text{asym}}$  shift, labeling coefficient, spillover factor and relaxation effects, we found that APT MRI showed significantly reduced heterogeneity between the brain gray matter and white matter yet it still clearly defined pH deficit within the ischemic lesion, which remains promising for clinical APT MRI (Sun et al., 2010). Importantly, we used relatively weak RF irradiation to capture pH-dependent APT contrast, which is approximately the optimal RF power level for in vivo APT imaging at 4.7 T (Sun et al., 2007b). Because the coupling between APT and MT effects should be relatively small at such a weak RF power level, our modeling of in vivo  $\text{MTR}_{\text{asym}}$  as a linear superposition of pH-dependent APT contrast and concomitant MT offset should be reasonably accurate (Sun, 2010; Zaiss et al., 2011). Moreover, our study used an unevenly-segmented RF irradiation scheme that enables multi-slice APT MRI with improved sensitivity (Sun et al., 2011a). Our study, therefore, complements and enhances the original work of Zhou et al. (Zhou et al., 2003).

Several studies have shown that APT MRI contrast, particularly  $T_1$ -normalized APT contrast, is capable of detecting ischemic tissue acidification (Jokivarsi et al., 2007; Katsura et al., 1991; Sun et al., 2011b). Here, we solved the confounding  $\Delta\text{MTR}'_{\text{asym}}$  and calibrated tissue pH, which may improve our mechanistic understanding of tissue acidification and associated damage mechanisms. Indeed, pH MRI showed graded pH deficit within the diffusion lesion. Whereas in vivo APT MRI contrast has been largely attributed to the intracellular compartment, Kintner et al. showed that intracellular and extracellular pH quickly equilibrate after an initial brief buffering phase that delays the sudden change in intracellular pH (Kintner et al., 1999). Hence, for the case of acute ischemic stroke, endogenous APT MRI captures an equilibrated intracellular and extracellular pH. Because the typical in vivo APT MRI contrast is about 2–3%, our study used an actively decoupled RF coil setup so both homogeneous  $B_1$  field and high sensitivity can be obtained (Sun et al., 2011b). We also used high-order Fastmap (Bruker Biospec, Billerica, MA) for shimming and PRESS without water suppression for adjusting the water frequency. The typical field inhomogeneity in the brain was within  $\pm 10$  Hz. This is consistent with the observation that the contralateral brain  $\text{MTR}_{\text{asym}}$  was  $-4.3 \pm 0.3\%$ , with a coefficient of variation of 7.2%. As such, field inhomogeneity correction algorithms were not necessary in our study (Kim et al., 2009; Sun et al., 2007a). Because the space between transmitter volume coil, surface

receiver coil and the animal brain is very limited, no phosphorus ( $^{31}\text{P}$ ) coil can be accommodated. We estimated tissue pH from quantitative lactate MRS, following the work of Chang et al., who obtained both  $^{31}\text{P}$  and  $^1\text{H}$  MRS, and showed strong correlation between lactate concentration and tissue pH during permanent ischemic stroke (Chang et al., 1990). Because pH may be dissociated from lactate concentration during sub-acute stroke phase and reperfusion, we studied hyper-acute stroke approximately 1 hr after MCAO to minimize such confounding factors (Jokivarsi et al., 2007; Morikawa et al., 1996). In fact, pH values derived from APT MRI is in very good agreement with literature values (Höhn-Berlage et al., 1989; Hugg et al., 1992; Komatsumoto et al., 1987; Smith et al., 1990).

It is important to point out that we proposed to use  $R_{1w}$ -scaled  $\Delta\text{MTR}'_{\text{asym}}$  map instead of a single global  $\Delta\text{MTR}'_{\text{asym}}$  value to compensate for MT asymmetry offset. It has been shown that the longitudinal relaxation rate is closely associated with magnetization transfer effect (Wolff and Balaban, 1989). Particularly, Li et al. showed that  $R_{1w}$  increases linearly with the concentration of cross-linked bovine serum albumin (Li et al., 2010). Their in vivo data at 9.4 Tesla also suggest that the product of macromolecule fraction ratio ( $p_m$ ) and exchange rate ( $k_{mf}$ ) approximately scales with  $R_{1w}$  in live rat brain. For instance,  $p_m * k_{mf} / R_{1w}$  calculated from Table 2 of Ref (Li et al., 2010) was 3.35 and 3.03 for brain WM and GM, within 10% from each other. Similar results were found from the study of Stanisiz et al. at 3 Tesla, with  $p_m * k_{mf} / R_{1w}$  being 3.47 and 3.64 for brain WM and GM, respectively (Stanisiz et al., 2005). Motivated by these findings, we numerically solved ROI-based  $\Delta\text{MTR}'_{\text{asym}}$  from striatum, and then derived a  $\Delta\text{MTR}'_{\text{asym}}$  map by scaling it with the experimentally obtained  $R_{1w}$  map. This approach significantly improved the homogeneity in APT images over the contralateral normal brain when compared with the conventional correction of a single global  $\Delta\text{MTR}'_{\text{asym}}$  value (Zhou et al., 2003). However, quantitative MT is somewhat challenging and additional study is needed to evaluate this approach in whole brain imaging. For instance, from the study of Sled et al. we estimated  $p_m * k_{mf}$  to be  $0.40 \pm 0.21$  with a coefficient of variance (CV) of 52% from twelve brain regions at 1.5 Tesla (Sled et al., 2004). In comparison,  $p_m * k_{mf} / R_{1w}$  was found to be  $0.24 \pm 0.09$  with its CV reduced to 36%. Whereas the proposed  $R_{1w}$ -scaled compensation algorithm does not eliminate the concomitant MT effect, it provides a first order correction of the heterogeneous MT effects. In summary, our work of quantitative pH imaging provides an imaging-based assessment of tissue acidosis and metabolic disruption, which may enable us to examine whether heterogeneous tissue outcome can be more accurately predicted with the inclusion of tissue pH, a surrogate metabolic marker, to the multi-parametric MRI analysis (Jacobs et al., 2001; Shen et al., 2005; Wu et al., 2007).

## 5. Conclusions

Our study elucidated concomitant RF irradiation effects and quantified endogenous APT MRI for absolute tissue pH. We showed that the severity and extent of ischemic tissue acidosis can be characterized using the proposed pH imaging, which may help improve our mechanistic understanding of tissue acidosis and metabolic disruption, as well as provide complementary information to conventional stroke MRI for improved characterization of ischemic tissue damage.

## Acknowledgments

This study was supported in part by grants from AHA/SDG 0835384N, NIH/NIBIB 1K01EB009771, NIH/IR21NS061119 and NIH/NCRR-P41RR14075. The authors would like to thank Ms. Nichole Eusemann for editorial assistance and Ms. Dominique Jennings for proof reading the manuscript.

## References

- Alsop DC, Detre JA. Multisection cerebral blood flow MR imaging with continuous arterial spin labeling. *Radiology*. 1998; 208:410–416. [PubMed: 9680569]
- Astrup J, Siesjo BK, Symon L. Thresholds in cerebral ischemia - the ischemic penumbra. *Stroke*. 1981; 12:723–725. [PubMed: 6272455]
- Bolas NM, Rajagopalan B, Mitsumori F, Radda GK. Metabolic changes during experimental cerebral ischemia in hyperglycemic rats, observed by 31P and 1H magnetic resonance spectroscopy. *Stroke*. 1988; 19:608–614. [PubMed: 3363594]
- Chang L, Shirane R, Weinstein PR, James TL. Cerebral Metabolite Dynamics during Temporary Complete Ischemia in Rats Monitored by Time-Shared 1H and 31P NMR Spectroscopy. *Magn Reson Med*. 1990; 13:6–13. [PubMed: 2319935]
- Florian C, Williams S, Bhakoo K, Noble M. Regional and developmental variations in metabolite concentration in the rat brain and eye: a study using 1H NMR spectroscopy and high performance liquid chromatography. *Neurochem Res*. 1996; 21:1065–1074. [PubMed: 8897470]
- Hata R, Mies G, Wiessner C, Fritze K, Hesselbarth D, Brinker G, Hossmann KA. A Reproducible Model of Middle Cerebral Artery Occlusion in Mice: Hemodynamic, Biochemical, and Magnetic Resonance Imaging. *J Cereb Blood Flow Metab*. 1998; 18:367–375. [PubMed: 9538901]
- Höhn-Berlage M, Okada Y, Kloiber O, Hossmann KA. Imaging of brain tissue pH and metabolites. A new approach for the validation of volume-selective NMR spectroscopy. *NMR Biomed*. 1989; 2:240–245. [PubMed: 2701807]
- Hossmann KA. Viability thresholds and the penumbra of focal ischemia. *Ann Neurol*. 1994; 36:557–565. [PubMed: 7944288]
- Hua J, Jones CK, Blakeley J, Smith SA, van Zijl PCM, Zhou J. Quantitative description of the asymmetry in magnetization transfer effects around the water resonance in the human brain. *Magn Reson Med*. 2007; 58:786–793. [PubMed: 17899597]
- Hugg JW, Duijn JH, Matson GB, Maudsley AA, Tsuruda JS, Gelinas DF, Weiner MW. Elevated Lactate and Alkalosis in Chronic Human Brain Infarction Observed by 1H and 31P MR Spectroscopic Imaging. *J Cereb Blood Flow Metab*. 1992; 12:734–744. [PubMed: 1506441]
- Jacobs MA, Zhang ZG, Knight RA, Soltanian-Zadeh H, Goussev AV, Peck DJ, Chopp M. A model for multiparametric mri tissue characterization in experimental cerebral ischemia with histological validation in rat: part 1. *Stroke*. 2001; 32:943–949. [PubMed: 11283395]
- Jokivarsi KT, Gröhn HI, Gröhn OH, Kauppinen RA. Proton transfer ratio, lactate, and intracellular pH in acute cerebral ischemia. *Magn Reson Med*. 2007; 57:647–653. [PubMed: 17390356]
- Katsura K, Ekholm A, Anders B, Siesjo BK. Extracellular pH in the Brain During Ischemia: Relationship to the Severity of Lactic Acidosis. *J Cereb Blood Flow Metab*. 1991; 11:597–599. [PubMed: 1904880]
- Kidwell C, Alger J, Saver J. Evolving paradigms in neuroimaging of the ischemic penumbra. *Stroke*. 2004; 35:2662–2665. [PubMed: 15472112]
- Kim M, Gillen J, Landman BA, Zhou J, van Zijl PCM. Water saturation shift referencing (WASSR) for chemical exchange saturation transfer (CEST) experiments. *Magn Reson Med*. 2009; 61:1441–1450. [PubMed: 19358232]
- Kintner DB, Anderson ME, Sailor KA, Dienel G, Fitzpatrick JH Jr, Gilboe DD. In vivo microdialysis of 2-deoxyglucose 6-phosphate into brain: a novel method for the measurement of interstitial pH using <sup>31</sup>P-NMR. *J Neurochem*. 1999; 72:405–412. [PubMed: 9886094]
- Kloska SP, Wintermark M, Engelhorn T, Fiebach JB. Acute stroke magnetic resonance imaging: current status and future perspective. *Neuroradiology*. 2010; 52:189–201. [PubMed: 19967531]
- Komatsumoto S, Nioka S, Greenberg JH, Yoshizaki K, Subramanian VH, Chance B, Reivich M. Cerebral energy metabolism measured in vivo by 31P-NMR in middle cerebral artery occlusion in the cat--relation to severity of stroke. *J Cereb Blood Flow Metab*. 1987; 7:557–562. [PubMed: 3654795]
- Li K, Zu Z, Xu J, Janve VA, Gore JC, Does MD, Gochberg DF. Optimized inversion recovery sequences for quantitative T1 and magnetization transfer imaging. *Magn Reson Med*. 2010; 64:491–500. [PubMed: 20665793]

- Marks MP, Olivot JM, Kemp S, Lansberg MG, Bammer R, Wechsler LR, Albers GW, Thijs V. Patients with acute stroke treated with intravenous tPA 3–6 hours after stroke onset: correlations between MR angiography findings and perfusion- and diffusion-weighted imaging in the DEFUSE study. *Radiology*. 2008; 249:614–623. [PubMed: 18936316]
- Morikawa S, Inubushi T, Takahashi K, Ishii H, Shigemori S. Dissociation between lactate accumulation and acidosis in middle cerebral artery-occluded rats assessed by <sup>31</sup>P and <sup>1</sup>H NMR metabolic images under A 2-T magnetic field. *Magn Reson Imaging*. 1996; 14:1197–1204. [PubMed: 9065911]
- Moseley M, Kucharczyk J, Mintorovitch J, Cohen Y, Kurhanewicz J, Derugin N, Asgari H, Norman D. Diffusion-weighted MR imaging of acute stroke: correlation with T2-weighted and magnetic susceptibility-enhanced MR imaging in cats. *Am J Neuroradiol*. 1990; 11:423–429. [PubMed: 2161612]
- Mougin OE, Coxon RC, Pitiot A, Gowland PA. Magnetization transfer phenomenon in the human brain at 7 T. *NeuroImage*. 2010; 49:272–281. [PubMed: 19683581]
- Nicoli F, Lefur Y, Denis B, Ranjeva JP, Confort-Gouny S, Cozzzone PJ. Metabolic counterpart of decreased apparent diffusion coefficient during hyperacute ischemic stroke: a brain proton magnetic resonance spectroscopic imaging study. *Stroke*. 2003; 34:e82–87. [PubMed: 12817104]
- Parsons MW, Li T, Barber PA, Yang Q, Darby DG, Desmond PM, Gerraty RP, Tress BM, Davis SM. Combined <sup>1</sup>H MR spectroscopy and diffusion-weighted MRI improves the prediction of stroke outcome. *Neurology*. 2000; 55:498–506. [PubMed: 10953180]
- Paschen W, Mies G, Hossmann KA. Threshold relationship between cerebral blood flow, glucose utilization, and energy metabolites during development of stroke in gerbils. *Exp Neurol*. 1992; 117:325–333. [PubMed: 1397169]
- Pekar J, Jezzard P, Roberts DA, Leigh JS, Frank JA, Mclaughlin AC. Perfusion imaging with compensation for asymmetric magnetization transfer effects. *Magn Reson Med*. 1996; 35:70–79. [PubMed: 8771024]
- Rivers CS, Wardlaw JM, Armitage PA, Bastin ME, Carpenter TK, Cvorov V, Hand PJ, Dennis MS. Do Acute Diffusion- and Perfusion-Weighted MRI Lesions Identify Final Infarct Volume in Ischemic Stroke? *Stroke*. 2006; 37:98–104. [PubMed: 16322499]
- Schaefer PW, Ozsunar Y, He J, Hamberg LM, Hunter GJ, Sorensen AG, Koroshetz WJ, Gonzalez RG. Assessing Tissue Viability with MR Diffusion and Perfusion Imaging. *Am J Neuroradiol*. 2003; 24:436–443. [PubMed: 12637294]
- Schlaug G, Benfield A, Baird AE, Siewert B, Lovblad KO, Parker RA, Edelman RR, Warach S. The ischemic penumbra: Operationally defined by diffusion and perfusion MRI. *Neurology*. 1999; 53:1528–1537. [PubMed: 10534263]
- Shen Q, Ren H, Fisher M, Duong TQ. Statistical prediction of tissue fate in acute ischemic brain injury. *J Cereb Blood Flow Metab*. 2005; 25:1336–1345. [PubMed: 15829912]
- Siesjo BK. Pathophysiology and treatment of focal cerebral ischemia: Part I: Pathophysiology. *J Neurosurg*. 1992; 77:169–184. [PubMed: 1625004]
- Sled JG, Levesque I, Santos AC, Francis SJ, Narayanan S, Brass SD, Arnold DL, Pike GB. Regional variations in normal brain shown by quantitative magnetization transfer imaging. *Magn Reson Med*. 2004; 51:299–303. [PubMed: 14755655]
- Smith C, Thomas G, Kryscio R, Markesbery W. <sup>31</sup>P spectroscopy in experimental embolic stroke: correlation with infarct size. *NMR Biomed*. 1990; 3:259–264. [PubMed: 2092741]
- Stanisz GJ, Odobina EE, Pun J, Escaravage M, Graham SJ, Bronskill MJ, Henkelman RM. T1, T2 relaxation and magnetization transfer in tissue at 3T. *Magn Reson Med*. 2005; 54:507–512. [PubMed: 16086319]
- Sun PZ. Simplified and scalable numerical solution for describing multi-pool chemical exchange saturation transfer (CEST) MRI contrast. *J Magn Reson*. 2010; 205:235–241. [PubMed: 20570196]
- Sun PZ, Benner T, Copen W, Sorensen A. Early experience of translating pH-weighted MRI to image human subjects at 3 Tesla. *Stroke*. 2010; 41:S147–S151. [PubMed: 20876492]

- Sun PZ, Cheung JS, Wang E, Benner T, Sorensen AG. Fast multi-slice pH-weighted chemical exchange saturation transfer (CEST) MRI with unevenly segmented RF irradiation. *Magn Reson Med.* 2011a; 65:588–594. [PubMed: 20872859]
- Sun PZ, Cheung JS, Wang EF, Lo EH. Association between pH-weighted endogenous amide proton chemical exchange saturation transfer MRI and tissue lactic acidosis during acute ischemic stroke. *J Cereb Blood Flow Metab.* 2011b; 31:1743–1750. [PubMed: 21386856]
- Sun PZ, Farrar CT, Sorensen AG. Correction for artifacts induced by B0 and B1 field inhomogeneities in pH-sensitive chemical exchange saturation transfer (CEST) imaging. *Magn Reson Med.* 2007a; 58:1207–1215. [PubMed: 17969015]
- Sun PZ, Zhou J, Huang J, van Zijl P. Simplified Quantitative Description of Amide Proton Transfer (APT) Imaging During Acute Ischemia. *Magn Reson Med.* 2007b; 57:405–410. [PubMed: 17260362]
- Utting JF, Thomas DL, Gadian DG, Helliard RW, Lythgoe MF, Ordidge RJ. Understanding and optimizing the amplitude modulated control for multiple-slice continuous arterial spin labeling. *Magn Reson Med.* 2005; 54:594–604. [PubMed: 16086330]
- Warach S. Thrombolysis in stroke beyond three hours: Targeting patients with diffusion and perfusion MRI. *Ann Neurol.* 2002; 51:11–13. [PubMed: 11782978]
- Ward KM, Balaban RS. Determination of pH using water protons and chemical exchange dependent saturation transfer (CEST). *Magn Reson Med.* 2000; 44:799–802. [PubMed: 11064415]
- Wolff SD, Balaban RS. Magnetization transfer contrast (MTC) and tissue water proton relaxation in vivo. *Magn Reson Med.* 1989; 10:135–144. [PubMed: 2547135]
- Wu O, Sumii T, Asahi M, Sasamata M, Ostergaard L, Rosen BR, Lo EH, Dijkhuizen RM. Infarct prediction and treatment assessment with MRI-based algorithms in experimental stroke models. *J Cereb Blood Flow Metab.* 2007; 27:196–204. [PubMed: 16685257]
- Zaiss M, Schmitt B, Bachert P. Quantitative separation of CEST effect from magnetization transfer and spillover effects by Lorentzian-line-fit analysis of z-spectra. *J Magn Reson.* 2011; 211:149–155. [PubMed: 21641247]
- Zauner A, Daugherty W, Bullock M, Warner D. Brain oxygenation and energy metabolism: part I—biological function and pathophysiology. *Neurosurg.* 2002; 51:289–301.
- Zhou J, Payen JF, Wilson DA, Traystman RJ, van Zijl PC. Using the amide proton signals of intracellular proteins and peptides to detect pH effects in MRI. *Nat Med.* 2003; 9:1085–1090. [PubMed: 12872167]

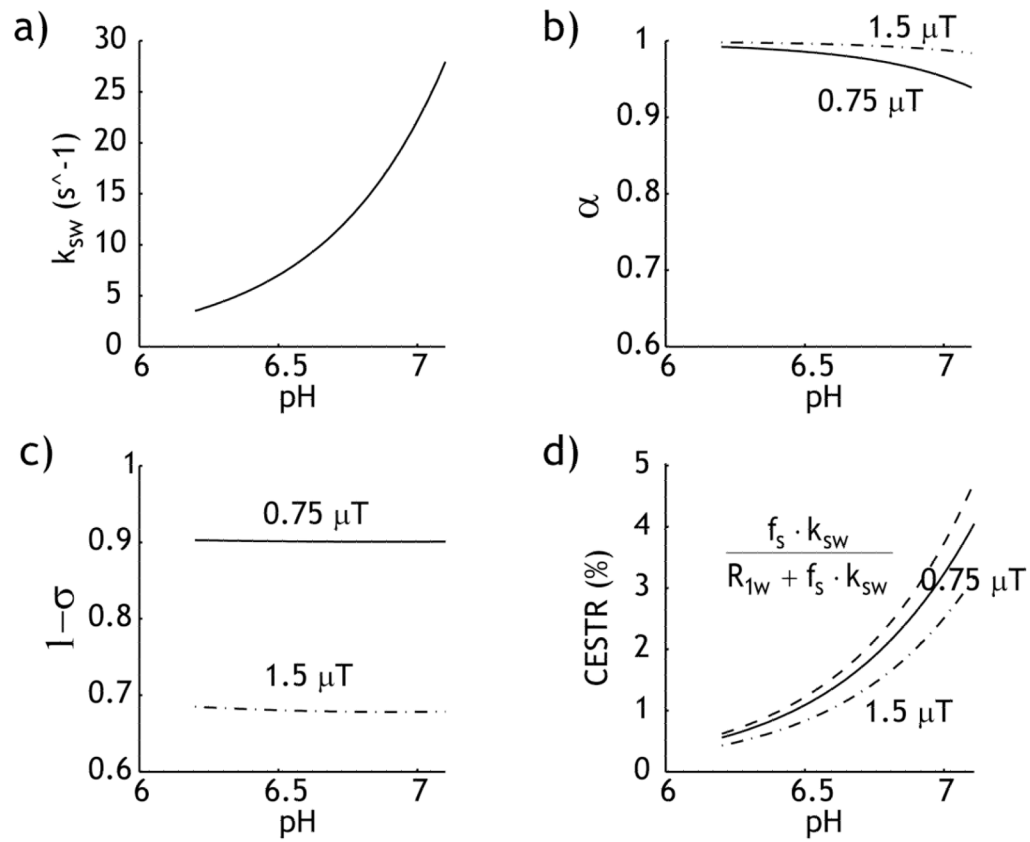


**Fig. 1.** pH-dependent amide proton CEST MRI. a) Base-catalyzed amide proton exchange rate as a function of pH  $k_{sw}=5.57 \times 10^{pH-6.4}$ . b) Labeling coefficient was calculated for a typical range of cerebral tissue pH. c) RF spillover factor degrades with RF power level. d) Comparison of the simplistic prediction (dashed,  $\alpha=1$  and  $\sigma=0$ ) and calculated CEST contrast under two representative RF power levels, 0.75 (solid) and 1.5  $\mu$ T (dash dotted).

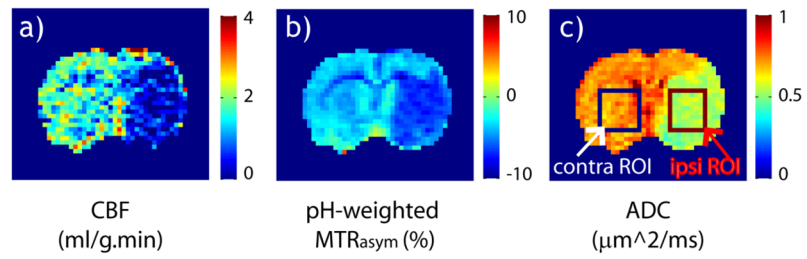


**Fig. 2.** Multi-parametric MRI of a representative acute ischemic stroke rat. Ischemic lesion displays significant deficit in CBF map (a), pH-weighted MTR<sub>asym</sub> map (b) and ADC map (c).

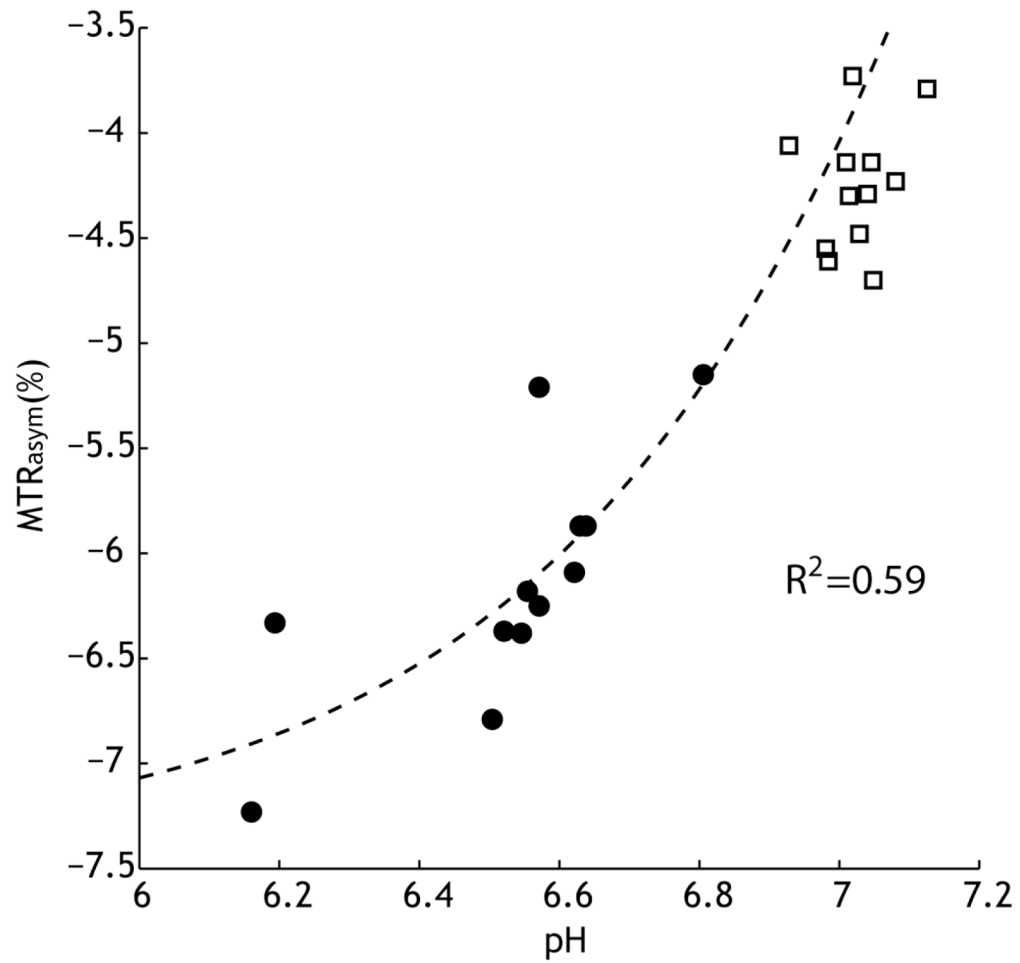


**Fig. 3.** *in vivo* MTR<sub>asyM</sub> is associated with tissue pH during acute stroke. MTR<sub>asyM</sub> can be described as a superposition of pH-dependent APT contrast (APTR) and MT asymmetry baseline shift ( $\Delta\text{MTR}'_{\text{asyM}}$ ). The labile amide proton concentration and  $\Delta\text{MTR}'_{\text{asyM}}$  were numerically solved from Eq.2, being 1/867 and  $-7.44\%$ , respectively. In addition, we calculated the contralateral normal tissue pH from quantitative APT MRI (Eq. 4), and overlaid its MTR<sub>asyM</sub> (open squares).

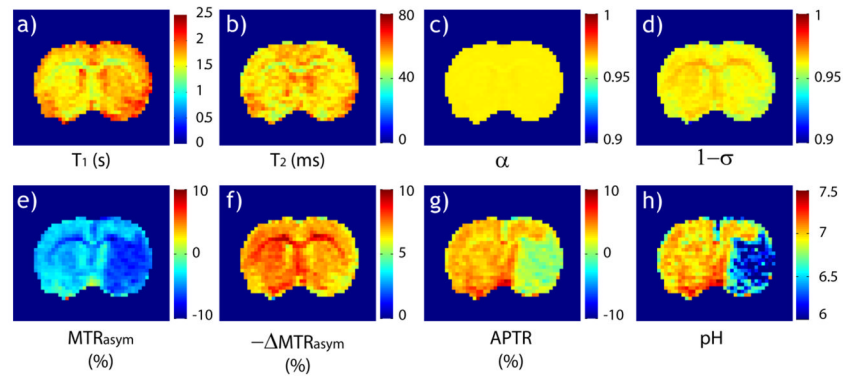


**Fig. 4.** Derivation of quantitative tissue pH from pH-weighted APT MRI. a)  $T_1$  map. b)  $T_2$  map. c) Estimated labeling coefficient map (assuming  $k_{sw}=20 \text{ s}^{-1}$  and  $B_1=0.75 \text{ } \mu\text{T}$ ). d) Estimated spillover factor map. e) pH-weighted  $MTR_{\text{asym}}$  map. f) Experimentally derived  $-\Delta MTR_{\text{asym}}$  map. g) pH-weighted APT map. h) Tissue pH map derived from Eq. 4, which clearly depicts tissue acidosis within the ischemic lesion.

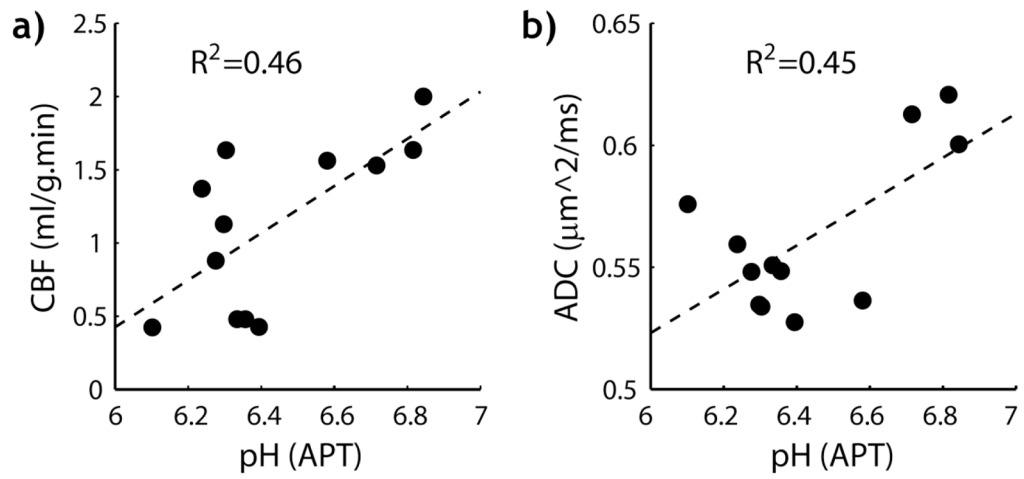


**Fig. 5.** Association between ischemic tissue pH and its perfusion and diffusion rates. a) Tissue pH correlated with residual CBF ( $R^2=0.46$ ,  $F<0.02$ ). b) Tissue pH increases with ADC ( $R^2=0.45$ ,  $F<0.02$ ).